Research Article

Youliang Cheng, Mingjie Wang, Changqing Fang*, Ying Wei, Jing Chen, and Jin Zhang

Variability and improvement of optical and antimicrobial performances for CQDs/mesoporous SiO_2/Ag NPs composites via *in situ* synthesis

https://doi.org/10.1515/gps-2021-0035
received February 01, 2021; accepted May 04, 2021

Abstract: To change the optical properties and improve the antibacterial performances of carbon quantum dots (CQDs) and Ag NPs, mesoporous SiO_2 spheres were combined with them to form the composites. In this paper, CQDs with a uniform size of about 3.74 nm were synthesized using glucose as carbon source. Then, CQDs/mesoporous SiO_2/Ag NPs composites were obtained *in situ* under UV light irradiating by using mesoporous SiO_2 and Ag NO_3 as the carrier and silver resource, respectively. The diameter of CQDs/mesoporous SiO_2/Ag NPs particles was in the range of 200–250 nm. With the increase in irradiating time, the red-shift in the UV-Vis spectrum for as-prepared CQDs/mesoporous SiO_2/Ag NPs composites was found, and the adsorption peak was widened. In addition, the composites showed a high antibacterial activity against *Staphylococcus aureus* and *Escherichia coli* via disc diffusion method. These results indicated that inhibition circles for Ag NPs/mesoporous SiO_2/CQDs and mesoporous SiO_2/Ag NPs were similar in diameter. Furthermore, the two composites had a better bactericidal performance compared with other particles. Therefore, as-prepared CQDs/mesoporous SiO_2/Ag NPs composites in this paper have great potential applications for fluorescent materials and antibacterial materials.

Keywords: silver nanoparticles, carbon quantum dots, mesoporous silicon dioxide, antimicrobial performances

1 Introduction

Raw materials of carbon quantum dots (CQDs) are very rich, and they showed low toxicity, good biocompatibility, multicolor fluorescence, excellent conductivity, and catalytic performances [1–6]. Compared with conventional semiconductor quantum dots, CQDs also had large specific surface area and exhibited strong fluorescence [7–10]. Moreover, CQDs, acting as both electron donors and electron acceptors, can be used as the oxidizer and reductant. Interestingly, the fluorescence for the system quenched when electron donor and acceptor were concurrent in the composites containing CQDs [11–13].

Ag NPs had excellent electrical and thermal conductivity, catalytic performances, antibacterial performances, and so on [14]. To the best of our knowledge, CQDs/Ag NPs composites are effective antibacterial materials in food packaging by using the synergistic effect of CQDs and Ag NPs. Besides, they can be applied in environmental protection and anti-counterfeiting [15]. Wang and coworkers synthesized core-shell structured CQDs/Ag NPs composites with the size of 40–80 nm, having a good monodispersity [16]. Zhao and coworkers prepared CQDs/Ag NPs composites consisting of CQDs well dispersed on the surface of Ag NPs [7]. For synthesizing CQDs/Ag NPs composites, reductants were essential, and surfactants were often used. As far as we know, the utilization efficiency would decrease drastically if materials had a poor stability [9]. Therefore, it is the key to control the stability of composites containing Ag NPs for building antibacterial materials [17].

Mesoporous SiO_2 particles had good optical transparency, biocompatibility, and high chemical inertness; thus, they were frequently used in preparing core-shell structured materials. Ge and coworkers synthesized mesoporous SiO_2 supported by Ag NPs and graphene quantum dots (GQDs), providing a highly reactive surface enhanced Raman scattering substrate [18]. Importantly, the solution

* **Corresponding author: Changqing Fang,** Faculty of Printing, Packaging Engineering and Digital Media Technology, Xi'an University of Technology, Xi'an 710048, China, e-mail: fcqxaut@163.com, tel: +86-29-82312038, fax: +86-29-82312512
Youliang Cheng, Mingjie Wang, Ying Wei, Jing Chen, Jin Zhang: Faculty of Printing, Packaging Engineering and Digital Media Technology, Xi'an University of Technology, Xi'an 710048, China

of GQDs prepared by the electrochemical method can be used as the reductant for *in situ* synthesis of Ag NPs/GQDs composites under UV irradiating.

Inspired by aforementioned studies, mesoporous SiO_2 spheres were used to improve the stability of as-prepared CQDs in this paper. Meanwhile, CQDs/mesoporous SiO_2/Ag NPs composites were prepared by using CQDs as the reductant. Interestingly, compared with Ag NPs and CQDs, CQDs/mesoporous SiO_2/Ag NPs composites showed variable optical properties and excellent antibacterial performances.

2 Experimental

2.1 Materials

Glucose was purchased from Kemio (Tianjin) Chemical Reagent Co., Ltd. Ag NO_3 particles were obtained from North China Petrochemical Co., Ltd. CTAB was purchased from Tianjin Windward Chemical Reagent Co., Ltd. Urea was purchased from Tianjin Yongsheng Fine Chemical Co., Ltd. Glycerol was purchased from Tianjin Fuchen Chemical Reagent Factory. Tetraethyl orthosilicate (TEOS) was purchased from Bellevue Chemical Technology Co., Ltd. *Escherichia coli* (CGMCC 1.2463) and *Staphylococcus aureus* (CGMCC 1.2910) were provided by Shanghai Luwei Technology Co., Ltd. Nutrient AGAR, anhydrous ethanol, and potassium bromide were purchased from Aoboxing (Beijing) Biotechnology Co., Ltd, Tianjin Fuyu Fine Chemical Co., Ltd, and Tianjin Beilian Fine Chemicals Development Co., Ltd, respectively. Deionized water was used throughout the experiments.

2.2 Synthesis of CQDs

CQDs were prepared by using glucose as carbon source via a hydrothermal method. Briefly, 0.6 g of glucose was dissolved in 90 mL of deionized water, and the mixture was transferred to a 100 mL teflon-lined autoclave and heated at 180°C for 24 h. Then, the reactor was cooled to room temperature naturally. Finally, obtained mixtures were centrifuged at a speed of 10,000 rpm for 15 min, and the supernatant containing CQDs was taken for further use.

2.3 Synthesis of mesoporous SiO_2 and CQDs/mesoporous SiO_2

Mesoporous SiO_2 was prepared by sol-gel method. Typically, 1.2 g of CTAB was dissolved in 80 mL deionized water with stirring for 30 min at a speed of 200 rpm. Meanwhile, 13.824 g of urea was dissolved in 120 mL deionized water and then mixed with above solution of CTAB. The temperature was set to 85°C and the stirring rate was 100 rpm. After stirring for 15 min, 32 mL of glycerol and 9.2 mL of TEOS were added, and then still stirred overnight. Obtained mixtures were centrifuged at 6,000 rpm for 15 min, and the precipitate was washed thrice with ethanol and once with deionized water. The white product was dried at 80°C for 5 h and then calcined at 540°C for 4 h to obtain mesoporous SiO_2 spheres.

For synthesizing CQDs/mesoporous SiO_2 composites, 0.075 g of as-prepared mesoporous SiO_2 was added to 5 mL of above CQDs solution with stirring for 2 h. The mixtures were centrifuged and then dried in a vacuum oven at 80°C for 12 h to obtain CQDs/mesoporous SiO_2 composites.

2.4 Synthesis of CQDs/mesoporous SiO_2/Ag NPs

CQDs/mesoporous SiO_2/Ag NPs composites were prepared in a photochemical reactor. Briefly, 5 mg of $AgNO_3$, 10 mL of CQDs solution, and 10 mL of deionized water were mixed with stirring for 20 min, and then placed in the photochemical reactor under UV irradiating with the power of 200 W. The irradiating time was set as 10, 20, and 30 min, respectively, and different samples of CQDs/mesoporous SiO_2/Ag NPs composites were obtained.

2.5 Characterization

Morphologies of CQDs, CQDs/mesoporous SiO_2, and CQDs/mesoporous SiO_2/Ag NPs were observed by transmission electron microscope (TEM, JEOL-2010, Japan). The specimens for TEM were prepared by dropping the solution containing samples on a copper grid and dried under an infrared lamp. The structure of CQDs was investigated by an X-ray diffractometer (Shimadzu XRD-7000, Japan) in the scanning range of 10–80°. Functional groups for CQDs were characterized by a Fourier infrared spectrometer (FTIR, SHIMADZU 8400S, Japan) using potassium bromide as the matrix in the range of 500–4,000 cm^{-1}. Optical performances were investigated by using an UV-Vis spectrometer (SHIMADZU UV-1800, Japan) and a fluorescence spectrometer (HITACHI, F-4600, Japan), and the samples were diluted before testing. All measurements were performed at room temperature.

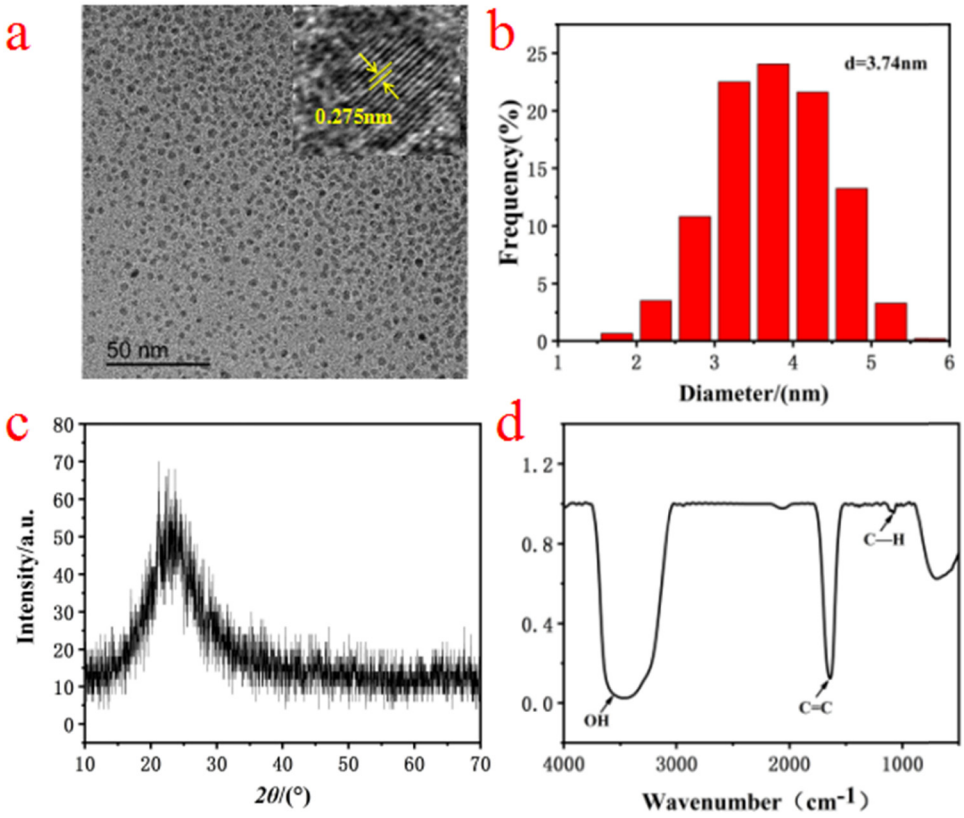

Figure 1: (a) TEM image of CQDs and high resolution image of single CQDs (upper right inset), (b) the size distribution graphics of CQDs, (c) XRD patterns of CQDs, (d) FTIR spectra of CQDs.

2.6 Antimicrobial test

Antibacterial effects of CQDs/mesoporous SiO_2/Ag NPs against *E. coli* and *S. aureus* were verified by the inhibition zone method. Briefly, 16.5 g of agar was dissolved in 500 mL deionized water at 100°C, and then 10–15 mL of agar solution was taken to drop to the petri dish. Meanwhile, *E. coli* and *S. aureus* were dissolved in sterile deionized water and diluted to make sure that the bacteria concentration was in the range of 10^6–10^8 cfu/mL. After the agar was solidified, an inoculating loop was used to scrape as-prepared *E. coli* and *S. aureus* solution and spread them on the solidified agar petri dish. Then, filter papers (the diameter of 6 mm) containing samples were placed on agar petri dishes. Finally, as-prepared petri dishes were put in a box (the temperature of 37°C and the humidity of 70%) for 24 h to observe the growth of bacteria around filter papers. All equipment in the experiment was sterilized and the whole process was operated under aseptic conditions.

3 Results and discussion

3.1 Morphologies and optical performances of CQDs and CQDs/mesoporous SiO_2 composites

TEM image of as-prepared CQDs is shown in Figure 1a, and they were near-spherical particles. In addition, the lattice spacing of (020) for CQDs (upper right inset in Figure 1a) was about 0.275 nm. According to Figure 1a, we counted the diameter of about 500 CQDs using Nano Measure software, and the size distribution is shown in Figure 1b. According to the result in Figure 1b, the particle size of most CQDs was in the range of 3–4 nm and the average diameter was about 3.74 nm. Thus, these results indicated that as-prepared CQDs with graphite like microcrystal had a small and relatively uniform size.

To further characterize the synthesized CQDs, as-prepared solution containing CQDs was freeze-dried, and

obtained solids were characterized by XRD. As shown in Figure 1c, there was a broad peak in the range of $2\theta = 20–30°$, indicating (002) lattice plane for synthesized CQDs. The FTIR spectrum for CQDs is shown in Figure 1d. The wide peak at 3,450 cm^{-1} was ascribed to the stretching vibration of –OH. In addition, the peaks at 1,600 and 1,100 cm^{-1} were attributed to the stretching vibration of C=C and the stretching vibration of C–H, respectively. These peaks corresponded to the characteristic functional groups for CQDs.

As shown in Figure 2a, as-prepared mesoporous SiO_2 spheres had a uniform size of about 200 nm. According to TEM image of CQDs/mesoporous SiO_2 composites (as shown in Figure 2b), we observed that CQDs were wrapped around SiO_2 by electrostatic interaction [19]. The illustration of the synthesis of CQDs/mesoporous SiO_2 composites is shown in Scheme 1.

To the best of our knowledge, CQDs usually exhibited characteristic absorption peaks in the range of 250–390 nm in UV-Vis spectra. As shown in Figure 3a, the UV-Vis absorption peak for CQDs located at around 260 nm because of the π–π* transition of C=C, while there were two peaks at around 290 and 400 nm for CQDs/mesoporous SiO_2 composites. The absorption peak at about 290 nm was because of the *n*–π* transition of C=O for CQDs in composites [20]. In addition, CQDs/mesoporous SiO_2 composites had a broad absorption line near 400 nm, which may be caused by the optical effect of mesoporous SiO_2 spheres [21,22].

According to the previous report, the fluorescence emission peak in the range of 300–500 nm belonged to the characteristic emission of CQDs [23]. As shown in Figure 3b, the strongest peak for CQDs was 375 nm at the excitation wavelength of 300 nm, and that for CQDs/mesoporous SiO_2 composites located at 365 nm. The latter containing CQDs with smaller size had a blue-shift, which was mainly attributed to the quantum size effect [24–26]. On the contrary, the intensity of fluorescence emission for the composites was greatly enhanced, which may be because of the reduction of surface defects for CQDs/mesoporous SiO_2, and the non-radiative transition also had less probability [27–30].

3.2 Morphologies and optical performances of CQDs/mesoporous SiO_2/Ag NPs

TEM images of CQDs/mesoporous SiO_2/Ag NPs obtained in photochemical reactor for different UV irradiating time are shown in Figure 4a–c. We found that the diameter of as-prepared Ag NPs was about 10 nm, and Ag NPs and CQDs mainly distributed on the surface of mesoporous

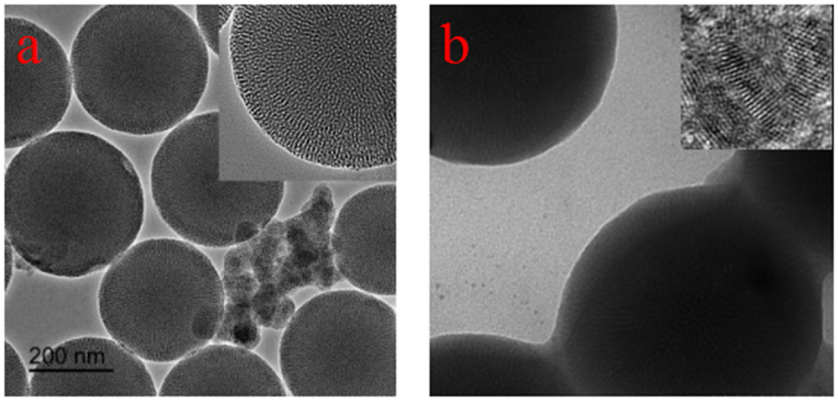

Figure 2: TEM images of (a) as-prepared mesoporous SiO_2 particles and (b) CQDs/mesoporous SiO_2 composites.

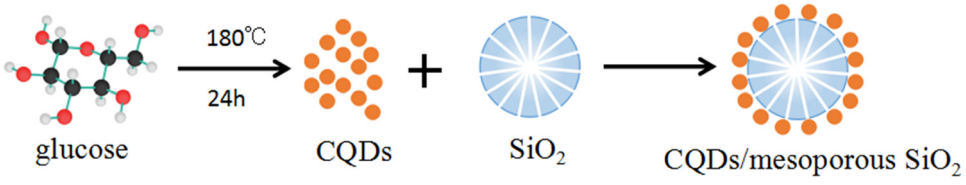

Scheme 1: Schematic diagram for the synthesis of CQDs/mesoporous SiO_2.

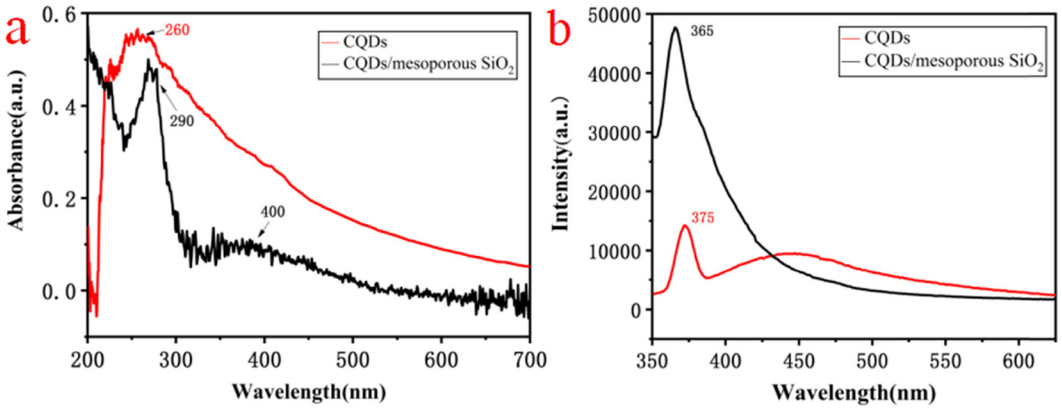

Figure 3: (a) UV-Vis spectra of CQDs and CQDs/mesoporous SiO_2, and (b) fluorescence emission spectra of CQDs and CQDs/mesoporous SiO_2.

SiO_2 spheres. Compared with Figure 4a, the particle size of Ag NPs as shown in Figure 4b and c was more uniform, and the amount changed to be more inferring that the concentration of obtained Ag NPs was higher under a longer UV irradiating time. These results indicated that the irradiation time plays an important role in the formation and the morphology of CQDs/mesoporous SiO_2/Ag NPs composites. The illustration of the formation of CQDs/mesoporous SiO_2/Ag NPs composites is shown in Scheme 2.

As shown in Figure 5a, the absorption peak of CQDs/mesoporous SiO_2/Ag NPs composites showed gradual blue-shift, and the absorption band was narrowed with the increase in UV irradiating time. This may be because of more uniform size and higher concentration of Ag NPs in the composite solution consistent with the result of TEM analysis [31].

Figure 5b shows that the wavelength for the fluorescence emission peak of composites basically remained constant. To the best of our knowledge, the wavelength of fluorescence emission for Ag nano clusters (Ag NCs) was around 530 nm, and the intensity was proportional to the concentration of Ag NCs in composites [32,33], similar to that obtained in this paper. In addition, there was a fluorescence emission peak at about 375 nm under the excitation wavelength of 300 nm, corresponding to the fluorescence emission peak of CQDs. This result was basically consistent with that in Figure 3b. As-prepared CQDs/mesoporous SiO_2/Ag NPs composites under UV irradiating for 30 min were selected as the specific sample for the antibacterial test because of the excellent optical performances.

3.3 Antibacterial performances of CQDs/mesoporous SiO_2/Ag NPs

The inhibition zones for as-prepared five antibacterial agents against *E. coli* and *S. aureus* are presented in Figure 6a and b, respectively. The initial concentration

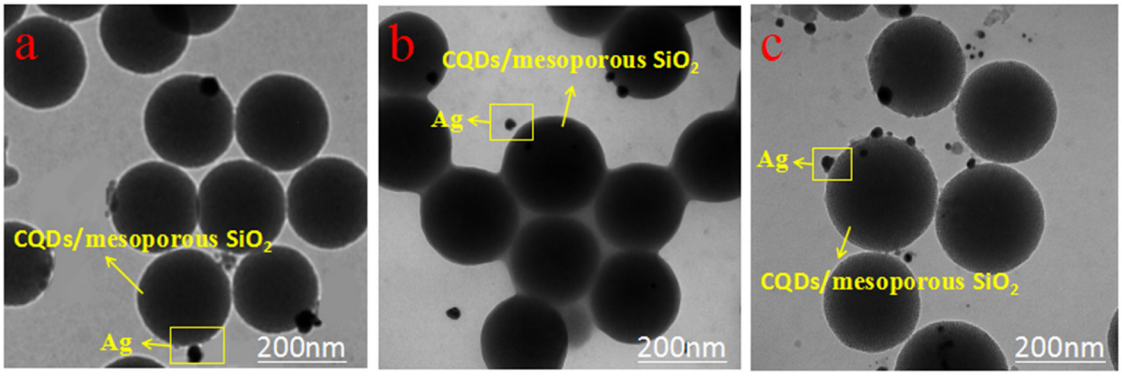

Figure 4: TEM images of CQDs/mesoporous SiO_2/Ag NPs composites in photochemical reactor for different UV irradiating time: (a) 1 h, (b) 2 h, and (c) 3 h.

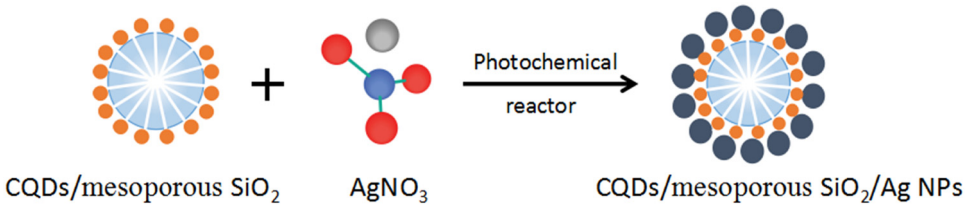

Scheme 2: Schematic diagram for the synthesis of CQDs/mesoporous SiO_2/Ag NPs.

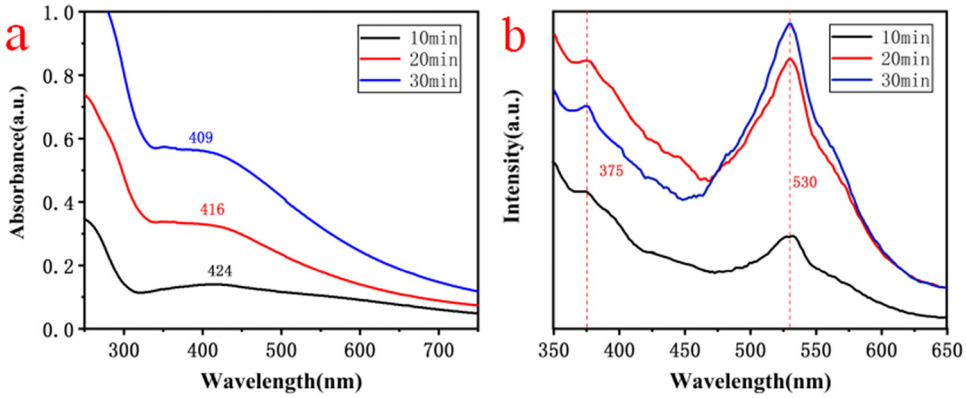

Figure 5: (a) UV-Vis spectra and (b) fluorescence emission spectra of as-prepared CQDs/mesoporous SiO_2/Ag NPs composites in photochemical reactor for different UV irradiating time.

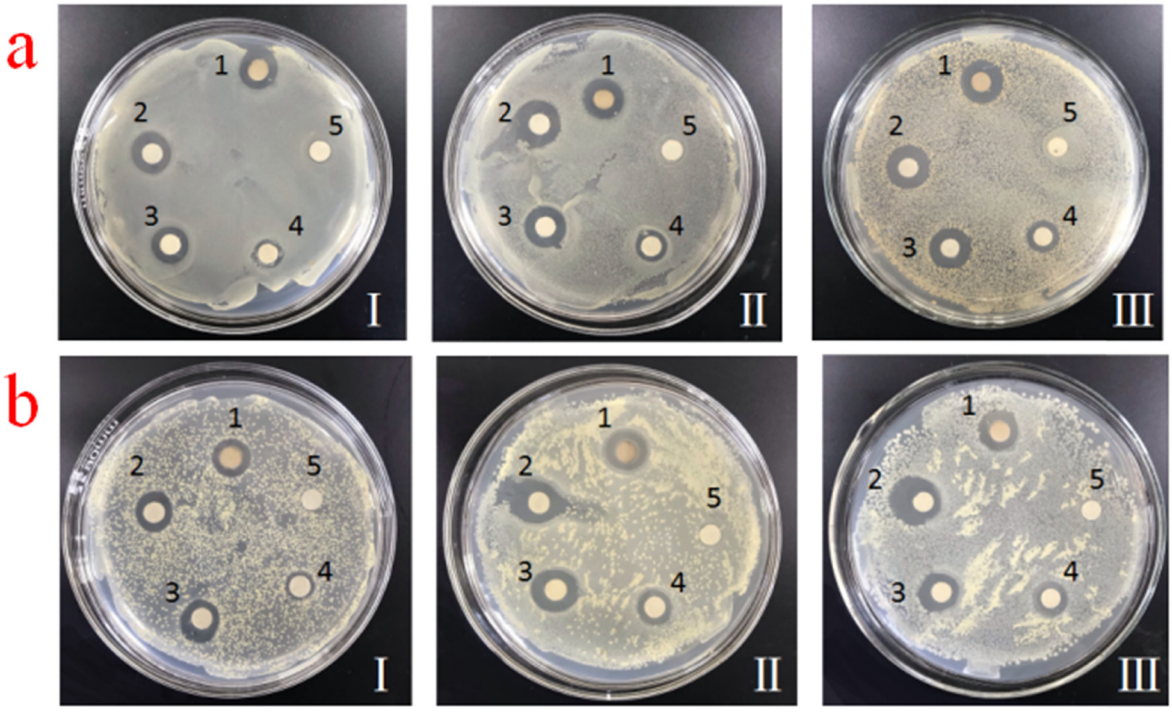

Figure 6: Representative images of agar plates containing (1) CQDs/mesoporous SiO_2/Ag NPs, (2) Ag NPs, (3) mesoporous SiO_2/Ag NPs, (4) CQDs/mesoporous SiO_2 and (5) CQDs, and inhibition zones for (a) *E. coli* and (b) *S. aureus* (diluted 10 times (I), 10^2 times (II), and 10^3 times (III), respectively).

of *E. coli* and *S. aureus* was diluted 10 times (I), 10^2 times (II), and 10^3 times (III), respectively. Antibacterial performances for these antibacterial agents were estimated by the size of inhibition zone. We found that CQDs/mesoporous SiO_2/Ag NPs and mesoporous SiO_2/Ag NPs composites showed excellent antibacterial performances against *E. coli* and *S. aureus*. To the best of our knowledge, sole Ag NPs possessed good antibacterial properties without any modification. The antibacterial mechanism for Ag NPs may be that Ag^+ on the surface of nanoparticles can interact with sulfhydryl and amino groups of DNA molecules; thus, bacteria cells failed to divide and proliferate and eventually die [34,35]. In addition, Ag NPs can be freely diffused into the culture medium and act as fungicides. In previous reports, CQDs have been used to synthesize the composites containing metal NPs and also can improve the stability of Ag NPs [36–39]. Ag^+ attached on mesoporous SiO_2 microspheres easily interacted with bacterial cells; therefore, CQDs/mesoporous SiO_2/Ag NPs and mesoporous SiO_2/Ag NPs composites also exhibited excellent antibacterial performances [40–42].

Compared with other samples, the antibacterial performance for solo CQDs was poor. However, that for CQDs/mesoporous SiO_2 was significantly improved by loading CQDs. According to the characteristics of composites, many –OH groups on the surface of mesoporous SiO_2 spheres have a strong activity. Therefore, they were used as carriers to adsorb antibacterial ions to achieve the sterilization [42,44]. Interestingly, the antibacterial activity of CQDs/mesoporous SiO_2/Ag NPs composites against *E. coli* was greater than that against *S. aureus*. This result may be because of the fact that Ag NPs eliminated the random distribution of DNA in *E. coli*, and the degradation of total DNA in *E. coli* was better than that in *S. aureus* [33,34]. According to the antibacterial effects against different dilutions of *E. coli* and *S. aureus*, we inferred that as-prepared composites can possess stable and effective antibacterial activity for *E. coli* and *S. aureus*.

4 Conclusion

In this work, glucose was used as the carbon source to synthesize CQDs via a hydrothermal method, and then mesoporous SiO_2 microspheres were used as carriers to prepare CQDs/mesoporous SiO_2/Ag NPs composites in a photochemical reactor. Compared with CQDs, optical properties of CQDs/mesoporous SiO_2/Ag NPs composites changed significantly, and the fluorescence intensity increased with the increase in UV irradiating time. In addition, mesoporous SiO_2/Ag NPs and CQDs/mesoporous SiO_2/Ag NPs composites showed a high stability and a strong antibacterial activity against both *E. coli* and *S. aureus*, which were similar to that for Ag NPs. Therefore, as-prepared CQDs/mesoporous SiO_2/Ag NPs composites in this paper can be used as potential candidate materials for antibacterial packaging.

Acknowledgments: The authors thank Huan Li for assistance with the antibacterial experiment and Xi'an Jiaotong University for testing equipment support.

Funding information: This work was supported by the National Natural Science Foundation of China (Grant No. 51772243), Key Research and Development Plan of Shaanxi Province (Grant No. 2020GXLH-Z-031), Weinan Industrial Innovation Project (Grant No. 2020ZDYF-GYCX-107), Xi'an Science and Technology Project (Grant No. 2020KJRC0074), and Key Scientific Research Project of Education Department of Shaanxi Province (Grant No. 20JS106).

Author contributions: Youliang Cheng: conceptualization, writing – review and editing, funding acquisition; Mingjie Wang: writing – original draft, data curation, investigation; Changqing Fang: resources, project administration; Ying Wei: investigation, validation; Jing Chen: supervision; Jin Zhang: supervision.

Conflict of interest: The authors state no conflicts of interest.

References

[1] Laux P, Tentschert J, Riebeling C, Braeuning A, Creutzenberg O, Epp A, et al. Nanomaterials: certain aspects of application, risk assessment and risk communication. Arch Toxicol. 2018;92(1):121–41.
[2] Goud KY, Reddy KK, Satyanarayana M, Kummari S, Gobi KV. A review on recent developments in optical and electrochemical aptamer-based assays for mycotoxins using advanced nanomaterials. Microcim Acta. 2019;187(1):1–32.
[3] Chandra S, Pathan SH, Mitra S, Modha BH, Goswami A, Pramanik P. Tuning of photoluminescence on different surface functionalized carbon quantum dots. RSC Adv. 2012;2(9):3602.
[4] Namdari P, Negahdari B, Eatemadi A. Synthesis, properties and biomedical applications of carbon-based quantum dots: an updated review. Biomed Pharmacother. 2017;87:20–2.
[5] Wang X, Cao L, Lu F, Mohammed JM, Li H, Qi G, et al. Photoinduced electron transfers with carbon dots. Chem Commun. 2009;46(25):37–74.

[6] Lu Q, Deng J, Hou Y, Wang H, Yao S. Hydroxyl-rich C-dots synthesized by a one-pot method and their application in the preparation of noble metal nanoparticles. Chem Commun. 2015;51:64–7.
[7] Zhao H, Guo Y, Zhu S, Song Y, Jin J, Ji W, et al. Facile synthesis of silver nanoparticles/carbon dots for a charge transfer study and peroxidase-like catalytic monitoring by surface-enhanced Raman scattering. Appl Surf Sci. 2017;410:42–50.
[8] Fernando K, Sahu S, Liu Y, Lewis KW, Guliants AE, Amirhossein J, et al. Carbon quantum dots and applications in photocatalytic energy conversion. ACS Appl Mater Inter. 2015;7(16):63–76.
[9] Sun YP, Zhou B, Lin Y, Wang W, Fernando KAS, Pathak P, et al. Quantum-sized carbon dots for bright and colorful photoluminescence. J Am Chem Soc. 2006;128(24):7756–7.
[10] Krysmann MJ, Kelarakis A, Dallas P, Giannelis EP. Formation mechanism of carbogenic nanoparticles with dual photoluminescence emission. J Am Chem Soc. 2012;134(2):747–50.
[11] Yong H, Chang YH, Song SH, Lee ES, Jin SH, Park C, et al. Intrinsic photoluminescence emission from subdomained graphene quantum dots. Adv Mater. 2016;28(26):5255.
[12] Qu D, Zheng M, Zhang L, Zhao H, Xie Z, Jing X, et al. Formation mechanism and optimization of high luminescent N-doped graphene quantum dots. Sci Rep. 2014;4(01):235–42.
[13] Wen ZH, Yin XB. Excitation-independent carbon dots, from photoluminescence mechanism to single-color application. RSC Adv. 2016;6(33):27829–35.
[14] Choi H, Ko SJ, Choi Y, Joo P, Kim T, Lee BR, et al. Versatile surface plasmon resonance of carbon-dot-supported silver nanoparticles in polymer optoelectronic devices. Nat Photonics. 2013;7(9):732–8.
[15] Lim SY, Shen W, Gao Z. Carbon quantum dots and their applications. Chem Soc Rev. 2015;44(1):362–81.
[16] Wang J, Gao XL, Sun HJ, Su B, Gao C. Monodispersed graphene quantum dots encapsulated Ag nanoparticles for surface-enhanced Raman scattering. ACS Mater. 2016;162:142–5.
[17] Chen JX, Fan LB, Yang CL, Wang SC, Zhang M, Xu J, et al. Facile synthesis of Ag nanoparticles-loaded chitosan antibacterial nanocomposite and its application in polypropylene. Int J Biol Macromol. 2020;161:1286–95.
[18] Ge J, Li Y, Wang J, Pu Y, Xue WD, Liu XG. Green synthesis of graphene quantum dots and silver nanoparticles compounds with excellent surface enhanced Raman scattering performance. J Alloys Compd. 2016;663:166–71.
[19] Cheng YL, Bai MS, Fang CQ, Yang MN. Preparation and characterization of water-soluble carbon quantum dots/mesoporous silica with high fluorescence intensity. Chem Lett. 2017;46(6):895–8.
[20] Sun S, Zhao S, Jiang K, Wang Y, Lin H. A facile approach to carbon dots-mesoporous silica nanohybrids and their applications for multicolor and two-photon imaging guided chemo-/photothermal synergistic oncotherapy. ChemNanoMat. 2020;6(6):953–62.
[21] Afonso D, Valetti S, Fraix A, Bascetta C, Petralia S, Conoci S, et al. Multivalent mesoporous silica nanoparticles photo-delivering nitric oxide with carbon dots as fluorescence reporters. Nanoscale. 2017;9(36):13404–8.
[22] Guo ZY, Zhu ZP, Zhang XG, Chen Y. Facile synthesis of blue-emitting carbon dots@mesoporous silica composite spheres. Solid State Sci. 2018;76:100–4.
[23] Wang MY, Xia YN, Qiu J, Ren XQ. Carbon quantum dots embedded mesoporous silica for rapid fluorescent detection of acidic gas. Spectrochim Acta A Mol Biomol Spectrosc. 2019;206:170–6.
[24] Wang Y, Suna A, McHugh J, Hilinski EF, Lucas PA, Johnson RD. Optical transient bleaching of quantum confined CdS clusters: The effects of surface trapped electron hole pairs. J Chem Phys. 1990;92(11):6927.
[25] Zhao S, Sun S, Jiang K, Wang Y, Liu Y, Wu S, et al. In situ synthesis of fluorescent mesoporous silica–carbon dot nanohybrids featuring folate receptor-overexpressing cancer cell targeting and drug delivery. Nanomicro Lett. 2019;11(02):193–205.
[26] Dong HN, Pang L, Wei Y, Cong HL, Shen YQ, Yu B. Preparation and application of carbon quantum dots filled hollow mesoporous silica nanospheres. Ferroelectrics. 2019;548(1):133–42.
[27] Tu YJ, Chen XM, Xiang YY, Yuan X, Ji X. Hydrothermal synthesis of a novel mesoporous silica fluorescence carbon dots and application in Cr(VI) and folic acid detection. Nano. 2020;15(7):2050090.
[28] Wang MY, Ren XQ, Zhu L, Xia Y, Qiu J. Preparation of mesoporous silica/carbon quantum dots composite and its application in selective and sensitive Hg^{2+} detection. Microporous and Mesoporous Materials. 2019;284:378–84.
[29] Dong YF, Ma JZ, Liu C, Bao Y. Ordered mesoporous silica encapsulated carbon quantum dots and its application in Fe^{3+} detection. Ceram Int. 2020;46(8):11115–23.
[30] Yang YH, Cui JH, Zheng MT, Hu CF, Tan SZ. One-step synthesis of amino-functionalized fluorescent carbon nanoparticles by hydrothermal carbonization of chitosan. ChemComm. 2012;48:380–2.
[31] Gyu RS, Irhas RA, My PPT, In I, Parket SY. Photoluminescence-tunable fluorescent carbon dots-deposited silver nanoparticle for detection and killing of bacteria. Mater Sci Eng C. 2019;97:613–23.
[32] Amjadi M, Abolghasemi-Fakhri Z, Hallaj T. Carbon dots-silver nanoparticles fluorescence resonance energy transfer system as a novel turn-on fluorescent probe for selective determination of cysteine. J Photoch Photobio A. 2015;309:8–14.
[33] Li WR, Xie XB, Shi QS, Duan SS, Ou-yang YS, Chen YB. Antibacterial effect of silver nanoparticles on Staphylococcus aureus. BioMetals. 2011;24(1):135–41.
[34] Li WR, Xie XB, Shi QS, Zeng HY, Ou-Yang YS, Chen YB. Antibacterial activity and mechanism of silver nanoparticles on Escherichia coli. Appl Microbiol Biotechnol. 2010;85(4):1115–22.
[35] Wei YL, Wang HF, Wang ZQ, Yu M, Chen S. Preparation and long-term antibacterial activity of TiO_2 nanotubes loaded with Ag nanoparticles and Ag ions. RSC Adv. 2015;91(5):74347–52.
[36] Feng T, Ai XZ, An GH, Yang P, Zhao Y. Charge-convertible carbon dots for imaging-guided drug delivery with enhanced in vivo cancer therapeutic efficiency. ACS Nano. 2016;10(4):4410–20.
[37] Miao P, Han K, Tang YG, Wang B, Lin T, Cheng W. Recent advances in carbon nanodots: synthesis, properties and biomedical applications. Nanoscale. 2015;5:1586–95.
[38] Meziani MJ, Dong X, Zhu L, Jones LP, LeCroy, Ethan G, et al. Visible-light-activated bactericidal functions of carbon quantum dots. ACS Appl Mater Interfaces. 2016;8:10761–66.

[39] Thakur M, Pandey S, Mewada A, Patil V, Khade M, Goshi E, et al. Antibiotic conjugated fluorescent carbon dots as a theranostic agent for controlled drug release, bioimaging, and enhanced antimicrobial activity. J Drug Deliv. 2014;2014:282193.
[40] Kovacova M, Markovic ZM, Humpolicek P, Micusik M, Švajdlenkova H, Kleinová A, et al. Carbon quantum dots modified polyurethane nanocomposites as effective photocatalytic and antibacterial agents. ACS Biomater Sci Eng. 2018;4(12):3983–93.
[41] Lv M, Su S, He Y, Huang Q, Hu WB, Li D, et al. Long-term antimicrobial effect of silicon nanowires decorated with silver nanoparticles. Adv Mater. 2010;22(48):5463–7.
[42] Lin L, Zhang HF, Cui HY, Xu M, Cao S, Zheng G, et al. Preparation and antibacterial activities of hollow silica–Ag spheres. Colloids Surf B. 2013;101:97–100.